

الهيئة الليبية للبحث العلمي

Libyan Authority For Scientific Research



(LIJNS)

Libyan International Journal of Natural Sciences

VOLUME 1 ISSUE 2 November 2025

Bi-Annual, Peer- Reviewed,
and Open Accessed e-Journal




Published by



MILJS@aonsrt.ly



Ion Acceleration from High Power Laser-Foil Interactions

^{1*} S. S. Abuazoum , Physics Department, Faculty of Science, Misurata University, Misurata, Libya

² K. Ledingham, Physics Department, Faculty of Science, Strathclyde University, Glasgow, U.K.

ARTICLE INFORMATION

Article history:

Received 22 August 2025

Accepted 21 September 2025

Published 26 September 2025

Keywords:

Laser-driven ion accelerators.

Heavy ions.

Ultrafast lasers.

High-peak-power.

Laser-plasma interaction

ABSTRACT

In this study, Multi-MeV ion and proton acceleration driven by the interactions of short (\sim ps) ultra-intense ($1 \times 10^{19} - 6 \times 10^{20} \text{ Wcm}^{-2}$) laser pulses with thin foil ($< 30 \mu\text{m}$) targets is experimentally investigated using the Vulcan Petawatt laser at the Rutherford Appleton Laboratory. It is found that for heavy ion emission, the ion cut-off energy scales with intensity, and that ion emission is seen coming from the edges of the foil targets. It is also found that a ring-shaped cold shockwave initiated in a thin foil target by a long-pulse laser beam resulted in a smooth and circular proton beam.

©Author(s) 2025. This article is distributed under the terms of the CC BY-NC 4.

1. Introduction

Ion acceleration produced by focusing a short high-intensity laser pulse onto a thin foil ($< 100 \mu\text{m}$) is a topic of intense experimental and theoretical interest internationally [1-4]. These ion beams are not accelerated directly by the laser pulse, instead they are indirectly accelerated by relativistic electrons generated by the laser-foil interaction over a gradient of the order of $\text{MeV}/\mu\text{m}$. Proton and ion beams generated this way have unique properties that make them attractive. These properties are a small source size ($\sim 100 \mu\text{m}$ scale), high brightness, and low divergence. Some of the possible applications of the ion beams generated in this way are proton imaging [5], medical isotope production [6-8], and laser-driven ion therapy [9, 10]. Also, in particle physics, high-energy heavy ion beams are widely used. Studies of collisions of heavy ions created by high-power laser-foil interactions at extremely high energies allow us to learn more about the structure of matter and the nature of the forces holding quarks in hadrons and the structure of particles like protons and neutrons [11].

This paper discusses the main research work on ion acceleration from high-power laser-foil interactions. The study centred on characterising ion and proton acceleration in terms of the laser parameters used. The study also focused on influencing laser-foil-generated ion beams by using low-temperature shocks in the foil.

2. Mechanism of Laser-Driven Acceleration of Ions

The most widely accepted scheme for accelerated ions of multi-MeV energies by a high-intensity laser is Target Normal Sheath Acceleration (TNSA) [12] at the back surface of the target foil. TNSA (shown in Fig. 1) works by first having electrons accelerated to relativistic speeds. This is done by the ponderomotive potential, U_{pond} of the laser's electric field acting on the plasma at the front surface of the foil, formed by the laser pre-pulse (amplified spontaneous emission). These electrons react to U_{pond} and are driven out from the high-intensity area which results in U_{pond} being converted into the relativistic kinetic energy of the electrons, K_e , see equation (1) [13].

* Corresponding author: E-mail addresses: saliazoum@gmail.com

$$U_{pond} \approx K_e = m_e c^2 \left(\sqrt{1 + \frac{\langle P^2 \rangle}{(m_e c)^2}} - 1 \right)$$

$$= m_e c^2 \left(\sqrt{1 + \frac{\langle e^2 E_0^2 \rangle}{2(m_e c \omega)^2}} - 1 \right) \quad (1)$$

where m_e is the electron mass, c is the speed of light, e is the electronic charge, E_0 is the magnitude of the electric field of the laser, and ω is the laser frequency. $\langle P^2 \rangle$ is the momentum imparted to an electron by the laser electric field, squared and averaged over the fast oscillations. Ions, on the other hand, have too high an inertia to be accelerated by this ponderomotive potential in the brief time that it exists. These relativistic electrons penetrate the foil, and when they exit the rear surface of the foil, they establish a strong space charge field (the sheath) of the order of TVm^{-1} . This electric field, E_{sheath} , can be estimated from the electron temperature (T_e) and density (n_e) using equation (2) [14].

$$E_{sheath} = \frac{K_b T_e}{e \lambda_D}, \quad \lambda_D = \sqrt{\frac{\epsilon_0 K_b T_e}{e^2 n_e}} \quad (2)$$

where ϵ_0 is the permittivity of free space and K_b is the Boltzmann constant. Atoms at the rear surface are ionised and accelerated by this field up to multi-MeV energies. The ions accelerated by this method depend on the contaminants present on the rear surface of the foil. Normally on the surfaces, there is water vapor and carbon-based compounds, which result in proton dominant acceleration due to the preferential acceleration of high charge-to-mass ratio ions. If the contaminants are removed by heating, ion bombardment or laser ablation, etc., then ions from the foil itself will be preferentially accelerated.

The ionisation mechanisms that occur during TNSA are believed to be collisional ionisation and field ionisation by barrier suppression. Ionisation due to the laser itself will not occur at the rear surface, due to it being absorbed by the front pre-plasma. Ionisation by shocks instigated in the foil by the pre-pulse will not generally happen due to the target thickness and density being sufficient to stop the shock break out. When a high temperature shockwave breaks out of the rear surface, it has been found that it switches off the TNSA mechanism due to rear surface disruption [15].

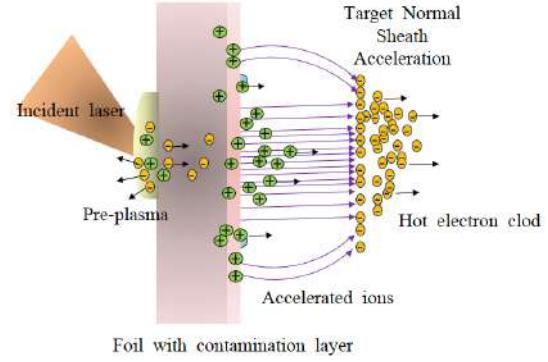


Fig. 1: TNSA mechanism summarises the acceleration process for multi-MeV ions due to an incident laser pulse (ultra-short and ultra-high intensity). The initial stage is pre-plasma expansion at the front surface due to heating from the laser pre-pulse. The next stage is then acceleration of electrons to relativistic speeds by the ponderomotive potential. The final stage is the establishment of the sheath electric field at the rear surfaces which then ionises and accelerates atoms to high energies.

3. Experimental set-up and results

The experiments presented here were performed at the Vulcan Petawatt laser system at the Central Laser Facility (CLF) of the Rutherford Appleton Laboratory (RAL). The high-power laser will be focused onto a thin foil, which enables TNSA to produce fast ions. The schematic setup is presented in Fig. 2. The Vulcan Petawatt laser can produce a beam with a wavelength of 1053 nm and an energy of up to 500 J in 500 fs. The energy delivered on the foil target is about a factor of 0.67 lower than what is measured before the final stage of chirped-pulse amplification (CPA) [17, 18] where the beam is compressed. The $f/3$ parabola was used to focus the laser down to peak intensities ranging from $1 \times 10^{19} \text{ Wcm}^{-2}$ to $6 \times 10^{20} \text{ Wcm}^{-2}$. The laser could be focused down to a focal spot of diameter $\sim 6 \mu\text{m}$, but for some shots, the laser was defocused on purpose to increase the focal spot size. The incident angle of the laser to the target normal was 45° .

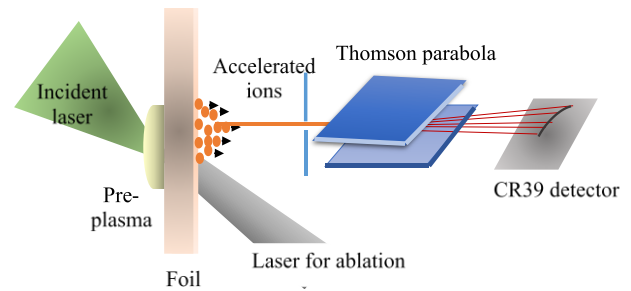


Fig. 2: Experimental arrangement for laser ion acceleration. A laser pulse is focused onto a thin metal foil. The ions accelerated from the target are dispersed with respect to energy and charge-mass ratio in a Thomson parabola, and then detected by nuclear track detector plastics (CR39).

The target foils used were 10 μm and 25 μm Al, Au, and Pd, which were resistively heated to $\sim 1000^\circ\text{C}$ during and 10 minutes before laser impact. Heating the targets removes the surface layers of water vapor and hydrocarbon compounds so that the heavier ions would be preferentially accelerated by the electron sheath. An ablation laser was also used to remove contaminants from the back surface of foils.

Many different techniques for the diagnostics of accelerated ions have been used in a number of experiments [1, 8, 16]. The only method used in the experiment for distinguishing ion species with differing charge-to-mass ratios and recording the energy spectra separately is given by two detectors, which consists of two parts: (1) Thomson parabola spectrometer, which uses parallel electric and magnetic fields to distinguish the ions due to their charge-to-mass ratio and energy. (2) Nuclear track detector (CR39) which uses to deliver information about impact numbers. It is attached to a base behind the Thomson parabola spectrometer. Every ion that impacts the CR39 damages the plastic, and when etched in concentrated NaOH solution, it results in pits on the plastic surface. The size of the pits and their spatial distribution are then recorded digitally using an automated microscope scanning system. The pit size depends heavily on the etching conditions of the CR39 and more weakly on the energy of the ion. The etching conditions found to be best for heavy ion detection are 6.25 M NaOH solution heated at 86°C with the CR39 being immersed for ~ 15 minutes. Using these etching conditions resulted in pit sizes varying between 1 and 20 μm in diameter, which could be identified by the scanning system but were not large enough to cause widespread saturation where pits merge together. The pit information for each parabola observed in the raw data was extracted, and the ion species identified. Then energy spectra for each ion were generated from the magnetic field deflection of the particle, this assumed an average magnetic field of 0.493 T. Pits were also sorted and colour coded for their size, defined by the major axis of the pit.

3.1 Ion acceleration characterisation by laser parameter variation

The effect of laser parameters on ion acceleration has been investigated. It was found that the maximum cut-off energies per nucleon of the ions observed, for the shots in the varying laser parameters data set, scaled with intensity. This is shown in Fig. 3, and it was also found to be true for the lower charge states. The target used during this data set was 25 μm Pd heated to 1000°C to remove contaminants.

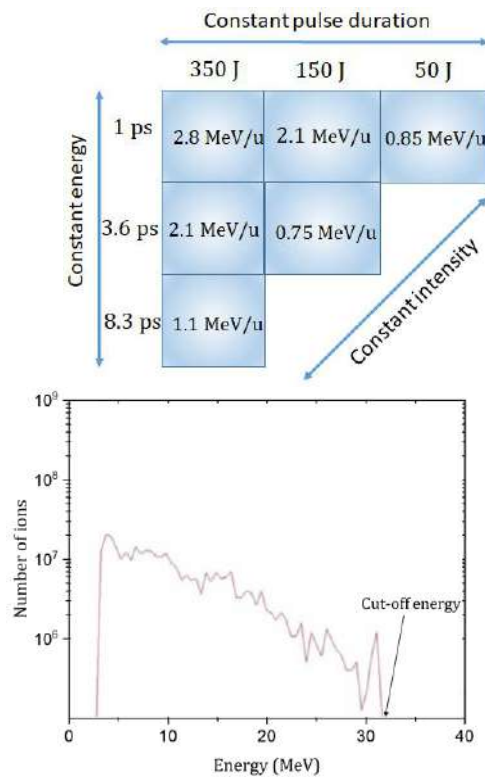


Fig. 3: The matrix on the top shows how the maximum cut-off energy per nucleon varies with the laser parameters. The graph is a typical energy spectrum for Pd charge state +7, laser energy 350 J, and pulse duration 3.6 ps, with a cut-off energy of 32 MeV.

3.2 Multiple source ion emission

To show the observation, an image of pits produced in a CR39 was optically scanned and illustrated in Fig. 4. It was observed on several shots that the source point, i.e. the point where neutral atoms (recombined ions) not deflected by the fields hit the CR39, was made up of several sources. For the on-axis rear-of-foil Thomson spectrometer, it was found that with a 50 μm pinhole it would act like a pinhole camera. The demagnification for this camera was calculated to be 0.47. The distance across the source on the CR39 is ~ 1.8 mm; this corresponds to the actual width (4 mm) of the target foil when taking into account the demagnification, see Figure 4c. For investigating the accelerated ion species from all of the source regions and looking for several ion tracks on the CR-39, the spatial resolution of the spectrometer was increased. Fig. 4a presents a spatial mapping of pits distributed in a full CR39 at higher resolution. By carbon ions from hydrocarbon contamination layers, the main tracks are produced. With higher spatial resolution, it was also found that different parabola would correspond to the same ion species but from different sources, this is observed in Fig. 4b. This implies that there is emission from the edges of the foil and corresponds to source 3 and 4 in

Fig. 4d. Source 1 corresponds to the most and highest charge states and so is likely to be the main emission from the foil. Source 2 is in the correct position and distance from the main source to correspond to this hole in the target. From all sources, the total recombined ion signal is $\sim 3\%$ of the overall ion signal produced on the CR39. With other estimates for similar experiments, this result is in good agreement [14]. Using a 340 J energy laser pulse focused to an intensity of $1 \times 10^{19} \text{ Wcm}^{-2}$, onto a heated Pd foil with a $50 \mu\text{m}$ diameter hole offset vertically $500 \mu\text{m}$ from the incident point of the laser, the measurement shown in Fig. 4 was obtained.

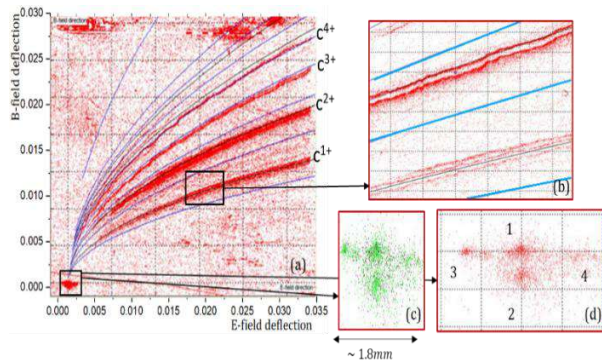


Fig. 4: (c) Optical image shows pits produced by neutral atoms in CR39. (a) Spatial mapping of pit distributions on a CR39, created by an automated scanning microscope. Carbon ions can be mainly observed in specific ion traces. (d) Magnified area for neutral atoms that remain undeflected within the fields of the spectrometer. At the center of the foil, Source areas are observed (1), at the edge of a $50 \mu\text{m}$ hole (2), and at the edges of the target, (3) and (4). (b) Magnified area displaying several tracks of carbon ion. All tracks originate from one of the four sources in (d).

3.3 Cold shock effects on laser-foil accelerated ion beams

The cold shock deforms the back surface of the foil target, locally shifting the foil normal axis and causing the ion beam to be diverted. To investigate the effects of long pulse (3- 6ns pulse length) initiated cold shocks on laser-foil accelerated proton and ion beams, two main diagnostics, a radio-chromic film (RCF) stack, and three Thomson spectrometers are used. For this investigation, three laser beams are used, one is the short pulse ($\sim 1 \text{ ps}$) which is used to generate the ion beam, and two long pulse beams ($\sim 3 \text{ ns}$ or $\sim 6 \text{ ns}$), which are used to cause cold shocks in the foil target. The short pulse enters the target vacuum chamber in the horizontal plane and is focused down onto the target using an $f/3$ parabola and a plasma mirror. The focal spot of the short pulse was measured to be $9 \pm 1 \mu\text{m}$. The long pulse beams are directly focused onto the target and enter the chamber at an angle of $\sim 25^\circ$ to the horizontal plane. At this angle, the long pulses are able

to reach the target by coming over the plasma mirror. The long pulse beams are focused by $f/10$ lenses outside the target chamber. The targets used were Cu foils with thicknesses of (5, 12.5, and $20 \mu\text{m}$). The range of intensities used for the short pulse is 1×10^{19} - $2.5 \times 10^{19} \text{ Wcm}^{-2}$. The plasma mirror [19, 20] is a block of glass that has an anti-reflection coating on its front surface. It works by transmitting the majority of the laser pre-pulse and when the main pulse starts to arrive, at intensities $> 10^{12} \text{ Wcm}^{-2}$ a plasma rapidly forms on the glass. This results in the main pulse of the laser being reflected with a much weaker pre-pulse, improving the laser pulse's contrast. Contrast is a term normally used to describe the quality of a laser in terms of its pre-pulse; this is the ratio between the amplitudes of the pre-laser pulse and the main pulse. The shape of the shocks initiated in the target by the long laser pulse beams was generated by modifying the shape of the long laser pulse focal spots, see Fig. 5.

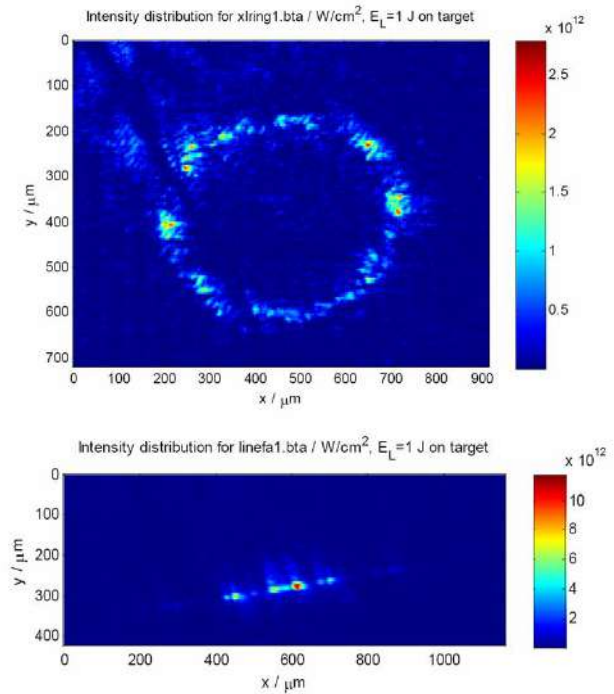


Fig. 5: This shows the two different shapes that the phase plates could alter the long pulse focal spot into.

The shock will take on the shape of the focal spot generating it so a ring focus would instigate a ring-shaped shock in the foil etc. The focal spot shape was altered using phase plates [21, 22] placed in the path of the long pulse beams. A phase plate causes the laser beam to interfere with itself so that constructive and destructive interference result in maxima and minima forming and so shaping the beam. The phase plates are designed to work so that the desired phase pattern is

formed at the focus of the laser beam. No obvious steering of the entire proton beam was observed when using either a ring or a line focus for the long pulse to generate a cold shock. It was observed that the line focus, used to generate a narrow shock across the width of the foil produces an asymmetry in the spatial d of the proton beam, see Fig. 6.

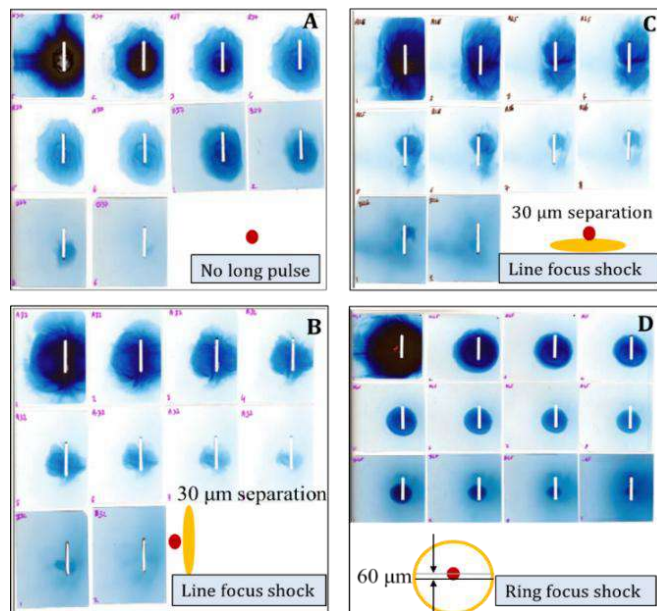


Fig. 6: Shown above are the scanned images of stack RCF from different long pulse focus shots for 5 μm Cu foils. Each piece corresponds to an energy slice of the proton beam. The yellow is the shape of the long pulse focus and the red dot is the relative position of the short pulse focal spot. (A) A typical proton beam spatial profile with increasing energy from 1-10. (B) A horizontal line focus placed 30 μm below the short pulse focal spot resulted in a vertical asymmetry to the spatial distribution. (C) A vertical line focus placed 30 μm to the side of the short pulse focal spot resulted in a horizontal asymmetry to the spatial distribution. (D) When the focal spot of a short laser pulse is placed within the circumference of a ring focus the result is a clean, circular and uniform proton beam. In D, the focal spot was positioned 60 μm above the center of the ring focus.

It is believed that the peak of the shock is splitting the area where TNSA is taking place, with a part of the lower energy proton source region being located on the opposite side of the shock peak to the rest of the source region. This also implies that the highest energy protons are being diverted off-axis. When using the ring focus it was found that a very smooth, circular, and clean proton beam distribution was produced, in agreement with Allen et al [23]. There was even an improvement with the thermal protons and ions on the first layer of RCF.

4. Conclusions

To conclude, the investigation of ion scaling with laser parameters found that the cut-off energies of heavy ion species, accelerated from thin foils by a short ultra-intense laser pulse, scale with intensity. Ion emission from the edges of foil targets was also diagnosed. The control and manipulation of the spatial profile of ion beams using secondary long-pulse laser beams was investigated. It was found that by using a ring-shaped cold shock, the quality of a proton beam could be improved, making the spatial distribution smoother and more circular.

Conflict of interest: The authors certify that there are no conflicts of interest.

Acknowledgments

The authors would like to acknowledge the scientific and technical expertise of the personnel at the Vulcan Laser Facility for their support during the course of this investigation.

References

- [1] E.L. Clark, K. Krushelnick, J.R. Davies, M. Zepf, M. Tatarakis, F.N. Beg, A. Machacek, P.A. Norreys, Measurements of energetic proton transport through magnetized plasma from intense laser interactions with solids. *Phys. Rev. Lett.* 84 (2000) 670-677. doi: org/10.1103/PhysRevLett.84.670
- [2] R. A. Snavely, M. H. Key, S. P. Hatchett, T. E. Cowan, M. Roth, T. W. Phillips, M. A. Stoyer, E. A. Henry, T. C. Sangster, M. S. Singh, S. C. Wilks, A. MacKinnon, A. Offenberger, D.M. Pennington, K. Yasuike, A.B. Langdon, B. F. Lasinski, J. Johnson, M. D. Perry, E. M. Campbell, Intense high-energy proton beams from petawatt-laser irradiation of solids. *Phys. Rev. Lett.* 85 (2000) 294-299. doi: org/10.1103/PhysRevLett.85.294.
- [3] J. Badziak, Laser-driven ion acceleration: Methods, challenges and prospects. *J. Phys. Conf. Series* 959 (2018) 201-206. doi: org/10.1088/1742-6596/959/1/201
- [4] B. Qiao, X.F. Shen, H. He, Y. Xie, H. Zhang, C.T. Zhou, S.P. Zhu, X.T. He, Revisit on ion acceleration mechanisms in solid targets driven by intense laser pulses. *Plasma Phys. Control. Fusion*, 61 (2019) 139-144. doi: org/10.1088/1361-6587/1/02/139
- [5] M. Borghesi, D. H. Campbell, A. Schiavi, M. G. Haines, O. Willi, A. J. MacKinnon, P. Patel, L. A. Gizzi, M. Galimberti, R. J. Clarke, F. Pegoraro, H. Ruhl, S. Bulanov, Electric field detection in laser-plasma interaction experiments via the proton imaging technique. *Phys. Plasmas* 9 (2002) 214-219. doi: org/10.1063/1.1459457
- [6] I. Spencer, K.W.D. Ledingham, R.P. Singhal, T. McCanny, P. McKenna, E.L. Clark, K. Krushe, Laser generation of proton beams for the production of short-lived positron emitting radioisotopes. *Nucl. Inst. Meth. B* 183 (2001) 449-458. doi: org/10.1016/S0168-583X(01)00771-6

- [7] S. Fritzler, V. Malka, G. Grillon, J. P. Rousseau, F. Burgy, E. Lefebvre, E. d. Humières, P. McKenna, K. W. D. Ledingham, Proton beams generated with high-intensity lasers: Applications to PET isotope production. *Appl. Phys. Lett.* 83 (2003) 3039-3041. doi: org/10.1063/1.1616661
- [8] K. W. D. Ledingham, P. McKenna, T. McCanny, S. Shimizu, J. M. Yang, L. Robson, J. Zweit, J. M. Gillies, J. Bailey, G. N. Chimon, High power laser production of short-lived isotopes for positron emission tomography. *J. Phys. D: Appl. Phys.* 37 (2004) 2341-2345. doi: org/10.1088/0022-3727/37/16/019
- [9] S.V.Bulanov, T.Z. Esirkepov, V.S. Khoroshkov, A.V. Kunetsov, F. Pegoraro, Oncological hadrontherapy with laser ion accelerators. *Physics Letters A* 299 (2002) 240-247. doi: org/10.1016/S0375-9601(02)00521-2
- [10] V. Malka, S.Fritzler, E.Lefebvre, E. dHumières, R. Ferrand, G. Grillon, C. Albaret, S.Meyroneinc, J. Chambaret, A.Antonetti, D. Hulin, Practicility of proton therapy using compact laser systems. *Medical Physics* 31, (2004) 1587-1592. doi: org/10.1118/1.1747751
- [11] J .Badziak, J.Domański, Acceleration of Heavy Ions by Ultrafast High-Peak-Power Lasers: Advances, Challenges, and Perspectives. *Photonics.* 12 (2025) 184-188. doi: org/10.3390/photonics12030184
- [12] S. C. Wilks, A. B. Langdon, T. E. Cowan, M. Roth, M. Singh, S. Hatchett, M. H. Key, D. Pennington, A. MacKinnon, R. A. Snavely , Energetic proton generation in ultra-intense laser-solid interactions. *Phys. Plasmas.* 8 (2001) 542 -548. doi: org/10.1063/1.1333697
- [13] B. M. Hegelich, Acceleration of heavy Ions to MeV/nucleon Energies by Ultrahigh-Intensity Lasers. Thesis at Ludwig Maximilian University of Munich, Germany (2002). doi: org/10.5282/edoc.660
- [14] M. Hegelich, S. Karsch, G. Pretzler, D. Habs, K. Witte, W. Guenther, M. Allen, A. Blazevic, J. Fuchs , MeV Ion Jets from Short-Pulse-Laser Interaction with Thin Foils. *Phys. Rev. Lett.* 89 (2002) 0850021-0850024. doi: org/10.1103/PhysRevLett.89.085002
- [15] D. Neely, P. Foster, A. Robinson, F. Lindau, O. Lundh, A. Persson, Enhanced proton beams from ultrathin targets driven by high contrast laser pulses. *Appl. Phys. Lett.* 89 (2006) 0215021-0215022. doi: org/10.1063/1.2220011
- [16] Allen, M. Laser Ion Acceleration from the Interaction of Ultra-Intense laser Pulse with thin foils. Thesis at Lawrence Livermore National Laboratory, USA (2004). doi: org/10.2172/15009814
- [17] Strickland, D. and Mourou, G. Compression of Amplified Chirped Optical Pulses. *Opt. Commun.* 56 (1985) 447-449. doi:org/10.1016/0030-4018 (85)90151-8
- [18] S.Backus, M.Margaret, M. Henry, C. Kapteyn, High Power ultrafast lasers. *Rev. Sci. Intr.* 69 (1998) 1207–1223. doi:org/10.1063/1.1148795
- [18] G. Doumy, F. Quéré, O. Gobert, M. Perdrix, P. Martin, P. Audebert, J.C. Gauthier, J.P. Geindre, Complete characterization of a plasma mirror for the production of highcontrast ultraintense laser pulses. *Physical Review E* 69 (2004) 026402. doi: org/10.1103/PhysRevE.69.026402
- [19] B. Dromey, S. Kar, M. Zepf, P. Foster, The plasma mirror-A subpicosecond optical switch for ultrahigh power lasers. *Rev. Sci. Instr.* 75 (2004) 645-649.
- [21] T.Boland, The Manufacture of Random Phase Plates and Phase Zone Plates, Central Laser Facility Annual Report (2020/2021) Rutherford Appleton Laboratory, UK
- [22] Burckhardt C. B. *Appl. Opt.* 9 (1970) 695-700. doi: org/10.1364/AO.9.000695
- [23] M. Allen, P. K. Patel, A. Mackinnon, D. Price, S. Wilks, E. Morse, Direct Experimental Evidence of Back-Surface Ion Acceleration from Laser-Irradiated Gold Foils. *Phys. Rev. Lett.* 93 (2004) 265004. doi: 10.1103/PhysRevLett.93.265004.